J. Anat. (2007) **210**, pp186–194 doi: 10.1111/j.1469-7580.2006.00680.x

Distinct developmental changes in the distribution of calcium, phosphorus and sulphur during fetal growth-plate development

C. C. van Donkelaar,[1] X. J. A. Janssen[2] and A. M. de Jong[2]

[1]*Department of Biomedical Engineering, and* [2]*Department of Applied Physics, Eindhoven University of Technology, The Netherlands*

Abstract

Gradients in the concentrations of free phosphate (Pi) and calcium (Ca) exist in fully developed growth zones of long bones and ribs, with the highest concentrations closest to the site of mineralization. As high concentrations of Pi and Ca induce chondrocyte maturation and apoptosis, it has been hypothesized that Ca and Pi drive chondrocyte differentiation in growth plates. This study aimed to determine whether gradients in the important spectral elements phosphorus (P), Ca and sulphur (S) are already present in early stages of development, or whether they gradually develop with maturation of the growth zone. We quantified the concentration profiles of Ca, P, S, chloride and potassium at four different stages of early development of the distal growth plates of the porcine femurs, using particle-induced X-ray emission and forward- and backward-scattering spectrometry with a nuclear microprobe. A Ca concentration gradient towards the mineralized area and a stepwise increase in S was found to develop slowly with tissue maturation. The increase in S co-localizes with the onset of proliferation. A P gradient was not detected in the earliest developmental stages. High Ca levels, which may induce chondrocyte maturation, are present near the mineralization front. As total P concentrations do not correspond with former free Pi measurements, we hypothesize that the increase of free Pi towards the bone-forming site results from enzymatic cleavage of bound phosphate.

Key words element mapping; embryonic bone development; epiphysis; fetal bone growth; particle-induced X-ray emission (PIXE).

Introduction

All longitudinal growth of long bones occurs in growth plates or at the growth fronts in the cartilaginous proximal and distal parts of the anlagen in fetal bones. Depending on the tissue under consideration, the majority of total longitudinal growth is due to cell hypertrophy (44–59% in 28-day-old rats), while the rest is due to matrix synthesis (28–40%) and proliferation (7–9%) (Wilsman et al. 1996). Although these proportions vary with species and animal age (Hunziker & Schenk, 1989), hypertrophy is generally considered to be the dominant factor in bone lengthening.

Numerous factors are known to be involved in chondrocyte maturation and hypertrophy. These include many proteins that control cell differentiation directly (see reviews by Kronenberg, 2003; Lefebvre & Smits, 2005) as well as factors that have an indirect effect via changes to the extracellular matrix. With regard to the latter, the stiffness of growth plate tissue is known to change with height (Fujii et al. 2000; Radhakrishnan et al. 2004). This is the result of changes in swelling pressure associated with the constitution of proteoglycans (Gakunga et al. 2000), which changes over the height of the growth plate (Shapses et al. 1994; Byers et al. 1997), in combination with changes in the collagen composition and the amount of collagen in the extracellular matrix (Wilsman et al. 1996; Noonan et al. 1998). The extracellular matrix is subject to degradation via

Correspondence
Dr C. C. van Donkelaar, Eindhoven University of Technology, Department of Biomedical Engineering, WH 4.118, PO Box 513, 5600 MB Eindhoven, The Netherlands. T: +31 40 2473135; F: +31 40 2447355; E: C.C.v.Donkelaar@tue.nl

Accepted for publication *27 September 2006*

matrix metalloproteinases (MMPs), expressed by hypertrophic chondrocytes in growth plates and early osteoarthritic cartilage (der Mark et al. 1992; Kirsch et al. 2000; Wu et al. 2002a; Ortega et al. 2004; Tchetina et al. 2005).

One way to induce terminal chondrocyte maturation and subsequent matrix mineralization is by exposing growth plate chondrocytes to high concentrations of inorganic phosphate (Pi) (Alini et al. 1994; Mansfield et al. 1999, 2001; Magne et al. 2003; Cecil et al. 2005). Pi uptake is mediated by sodium-dependent phosphate co-transporters present in growth plate chondrocytes (Wada et al. 2004; Wu et al. 2002b).

High concentrations of extracellular calcium (Ca) induce chondrocyte maturation *in vitro* (Bonen & Schmid, 1991) by enhancing the uptake of Pi (Mansfield et al. 2003) and by up-regulating the expression of several differentiation markers such as collagen type X, parathyroid hormone-related peptide (PTHrP) and matrix metalloproteinase-13 (MMP13) (Zuscik et al. 2002; Wu et al. 2004; Burton et al. 2005).

The findings that Pi and Ca lead directly and indirectly to chondrocyte maturation are especially relevant as Ca (Wroblewski, 1987; Mwale et al. 2002), Pi (Mwale et al. 2002) and phosphorus (P) (Wroblewski, 1987) gradients are known to exist in growth plates, with concentrations increasing towards the bone. It has been postulated that these gradients arise via diffusion from the remodelling of mineralized cartilage into mature bone. This leads to the tempting hypothesis that bone turnover stimulates ongoing cartilage mineralization.

However, if bone turnover is responsible for the existence of these Pi and Ca gradients, these gradients are unlikely to exist in the matrix before the first turnover of bone is present. If this is correct, Ca and P gradients are likely to develop with maturation of the growth zone.

The aim of this study was to assess quantitatively the hypothesis that gradients in Ca and P develop in the course of time, depending on the developmental stage of a long bone. Therefore, distributions of total Ca and P are determined at different stages of development of a growth plate. Additionally, the total amount of sulphur (S) is determined as a measure of the distribution of charged sulphated matrix components. Quantifying changes in these concentrations as a function of developmental stage is new. Also, quantitative concentration profiles of these elements are obtained at high spatial resolution using particle-induced X-ray emission (PIXE) measurements and forward and backward scattering spectrometry with a nuclear microprobe. The aforementioned studies used spot measurements (Wroblewski, 1987) or low-resolution profiles (Mwale et al. 2002).

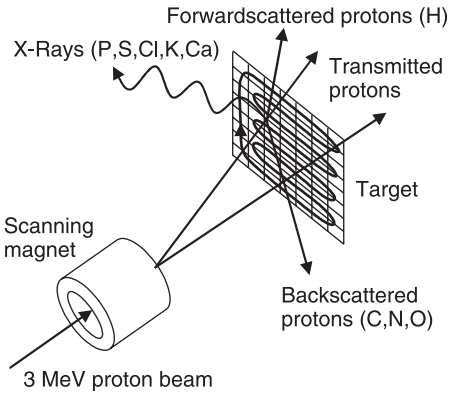

Fig. 1 Schematic principle of sample analysis with a nuclear microprobe: a high-energy proton beam is scanned across the sample in a two-dimensional grid. Upon interaction with the protons, two processes occur. First, X-rays are emitted from target atoms when hit by a proton. These X-rays are detected during the PIXE measurement. Second, transmitted protons are scattered from their straight path in either a forward (FS) or a backward (RBS) direction.

Materials and methods

The distribution of tissue elements was measured in a nuclear microprobe experiment. In this experiment a beam of high energy (typically several MeV) ions was scanned over a thin sample. The beam was focused on a small spot (a few square micrometres in size). From the interaction of the ions with the sample information was obtained from each position where the beam hits the sample. This resulted in a two-dimensional map of the elemental distribution. Ion beam analysis techniques are based on the interaction processes of highly energetic projectiles with matter (Fig. 1). If a thin sample is irradiated by a high-energy ion beam, the vast majority of ions travel through the sample while losing a small part of their energy. A fraction of the ions interact with the atoms in the sample in three ways: they can scatter from their original direction in backward or forward direction, or they can induce the emission of an X-ray photon (PIXE). These interactions are explained in more detail below.

PIXE is a very sensitive technique for the quantitative detection of elements with an atomic mass above 20,

such as calcium and phosphorus. The inner shells of the target atoms are ionized by the incident particles. During de-excitation of a vacancy in the inner shell of the atom an X-ray photon is emitted. The energy of the emitted photons depends on the element and shell and is typically in the range of 1–4 keV for the elements ranging from phosphorus to calcium. The photons are detected and the target element is identified by the measured photon energy. The concentrations of these elements can be determined if the total density of the material is known.

The quantities of hydrogen (H), carbon (C), nitrogen (N) and oxygen (O), which together make up most of the tissue density, are determined by simultaneous forward and backward scattering spectrometry. Scattering can take place in forward or backward direction, depending on the mass of the target atom on which the ion scatters. Rutherford backscattering (RBS) and forward scattering (FS) spectrometry rely on the detection of projectiles after scattering on target atoms (Chu et al. 1978). The target element is identified by the measured projectile energy. FS ($\theta = 45°$) was used to determine the amount of H in the sample, and RBS ($\theta = 147°$) the amount of C, N and O.

For the PIXE, FS and RBS measurements, a 3-MeV proton beam of 100 pA was generated in a Singletron™ (Mous et al. 1997) accelerator (High Voltage Engineering Europe), located at the Department of Applied Physics, Eindhoven University of Technology (Mutsaers et al. 1990). The experiments were performed at room temperature under high vacuum (8^{-10} mbar) in a chamber equipped with an ultralow-energy germanium X-ray detector (Canberra) and two passivated implanted planar silicon particle detectors (Canberra). The detectors were placed at angles of 135°, 45° and 147°, respectively, relative to the direction of the beam.

Two-dimensional information was obtained by scanning the beam with a spot size of 2 μm across the sample in a rectangular pattern of 120×32 pixels at a rate of 1000 pixels per second with a step-size of 10 μm and simultaneously recording the PIXE (Johansson, 1989; Isabelle, 1994; Traxel, 1998), FS and RBS data (Chu et al. 1978) and the position of the beam. These methods have been applied previously on articular cartilage (Reinert et al. 1998). The total measurement time of one measurement was 3 h, ensuring enough data was collected without inducing large radiation damage to the samples.

Fresh porcine embryos of different ages were obtained from a local abattoir within 1 h after slaughter of the sow. Femurs of four animals were selected such that the developmental stages of these bones were clearly different. The selected femurs were 2, 3, 6 and 8 cm long and will be referred to as specimens A, B, C and D, respectively. Based on femur lengths and crown–tail lengths the approximate embryonic ages of these specimens were estimated at 50, 60, 90 and 110 days, respectively. Their developmental stages were characterized by the appearance of distal epiphyses. In femur A the primary ossification centre had just developed. Hypertrophic chondrocytes were present around the primary ossification centre but not yet in the area where the secondary ossification centre develops at a later stage. Femur B showed a fully developed primary ossification centre but no secondary centre. Femur C contained the onset of a proximal secondary ossification centre. Femur D contained a fully developed secondary ossification centre.

Immediately after dissecting the femur, the proximal part of the bone was clamped in a processor-controlled circular saw (Accutom-5; Struers GmbH, Ballerup, Denmark) equipped with a diamond saw blade. The distal epiphysis with a small strip of underlying bone was sawn from the rest of the bone and frozen at −80 °C until further processing. Subsequently, 10-μm cryosections (Microm HM550) were obtained in the frontal plane. Sections for analysis of the elemental distribution were transferred to 100-nm-thick Formvar support films. These films were obtained as follows. A clean glass slide was coated with Formvar dissolved in chloroform. Chloroform evaporates quickly, leaving a film of Formvar behind. Films were transferred onto a thin plastic sheet with a 10-mm-diameter hole. Foils with homogeneous thickness of 100 nm exhibit a homogeneous gold-like colour as confirmed by optic profilometry. These films were selected and tested for fragments of glass or dust with light transmission and reflection microscopy. Subsequently, they were dried in a vacuum desiccator to avoid dust contamination, where they are kept until use.

After transferring the histological sections to the Formvar foils, the sections were kept at −20 °C for 1 h to dry without melting before storing them in a vacuum desiccator until analysis. The vacuum desiccation prevented re-absorption of moisture from the air and reduced the amount of water contained in the sections even further.

As an illustration of the data obtained from this measurement, raw data from a section that contains

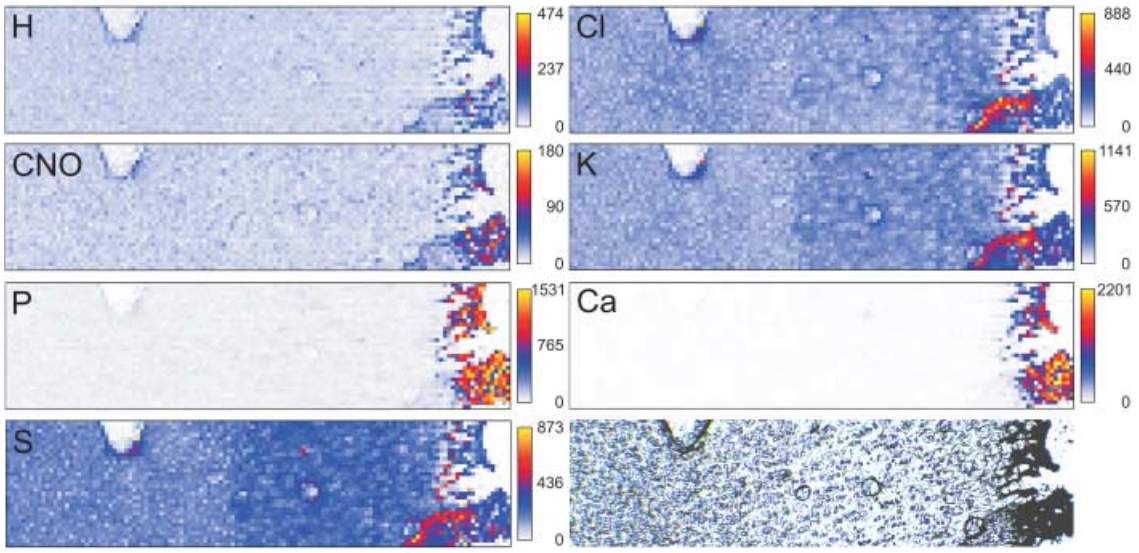

Fig. 2 Example of a raw data set, which contains some characteristics that can be used for orientation. These markers can clearly be traced in all raw images, illustrating the accuracy of the method. Note that such biasing aspects are not present in the actual measurements. Images are marked with the name of the element that is plotted. The image indicated with CNO contains the sum of all detected elements C, N and O. From blue to yellow, the amounts of detected elements increase. The bottom right image shows the unstained sample on Formvar foil.

some characteristic structures is shown in Fig. 2. A blood vessel, a circular irregularity due to sample preparation and a part of the section that was accidentally folded are visible in the histology section as well as in the elemental distributions. This sample was obtained from a pilot study and is provided here as an example. In the actual measurements areas were selected in which such irregularities were absent. This was confirmed by the absence of small regions with lower or higher intensity in the PIXE yield.

Absolute quantification requires that the raw data are corrected for self-absorption of X-rays in the sample and for the energy loss of particles while travelling through the sample (Brands et al. 1999). The actual concentrations of the elements in milligrams per gram dry weight (mg g^{-1} dw) measured with PIXE are determined by assuming that the amount of matrix elements (H, C, N and O) together with the total amount of PIXE elements (P, S, Cl, K and Ca) makes up 100% of the total local tissue mass. Without this correction at each measurement spot for tissue thickness and/or tissue density using H, C, N and O the eventual concentrations would be based on an estimated tissue density and on the assumption that the density is constant throughout the tissue. Not only does the total concentration of all elements depend on the tissue density, but also the ratio between concentrations of different elements depends on tissue density (Brands et al. 1999). Hence, neglecting the local tissue density may introduce non-existent spatial concentration gradients.

Finally, the two-dimensional mappings of the concentrations (mg g^{-1} dw) were averaged in the medio-lateral direction. This is permitted because in this direction the concentrations are assumed to be equal, as can also be derived from the mappings shown in the example (Fig. 2). These averaged data were used for further evaluation.

Results

The average concentrations of Ca, P, S, K and Cl as a function of distance from the primary ossification centre were determined for all four samples (Fig. 3). The locations at the end (Fig. 3A–D) and the beginning (Fig. 3D) where Ca and P increase several-fold indicate the transition between growth plate and mineralized tissue. The graphs show that a gradient in the calcium profile is not yet present in the youngest animal (Fig. 3A), but that this becomes more apparent when the age of the animal increases (Fig. 3B,C). In the oldest growth plate the gradient runs in both directions (Fig. 3D). None of the samples shows a gradient in P. The distribution of K follows that for S in all cases. As for Ca, a distinct distribution arises for S and K with

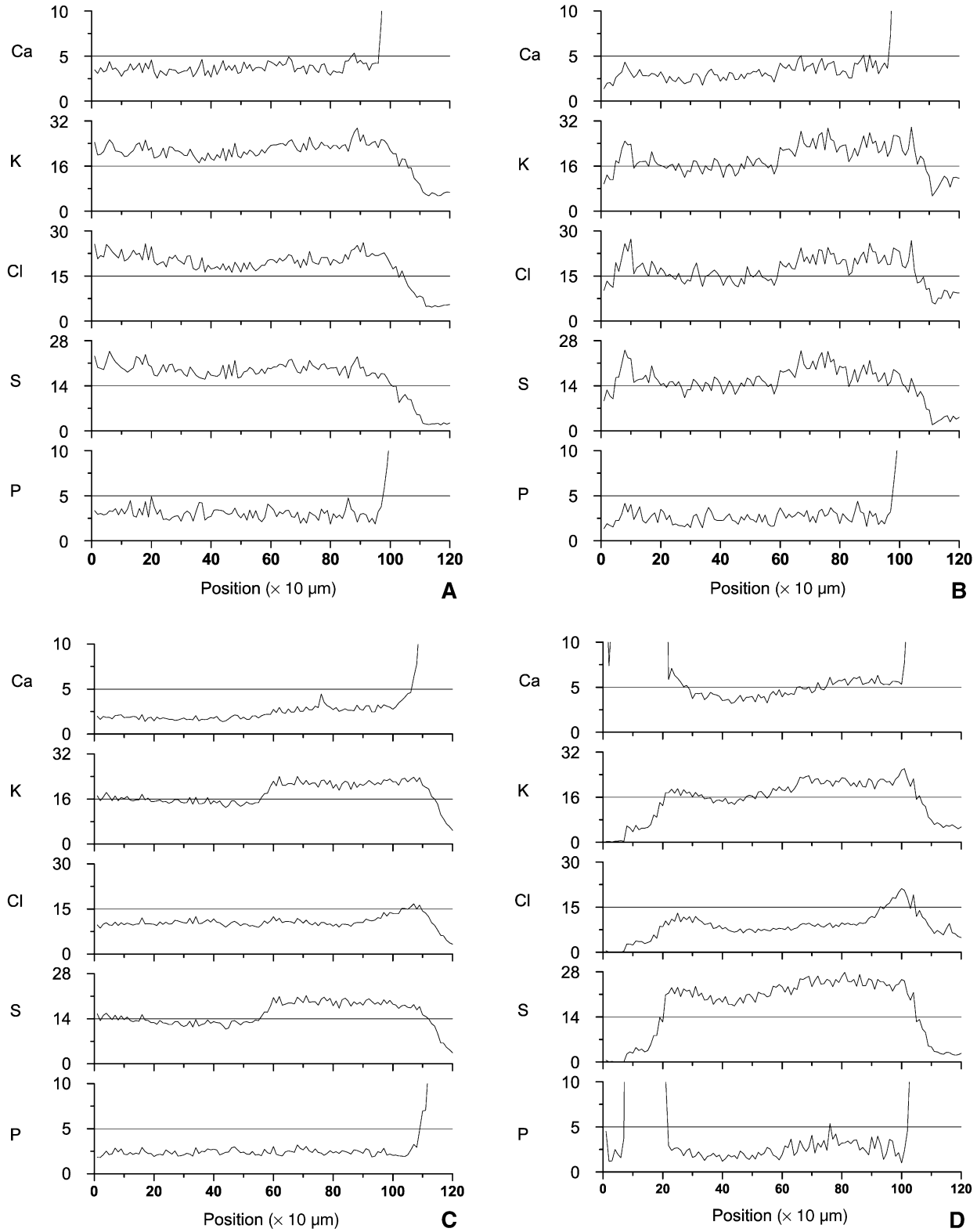

Fig. 3 Concentration profiles of Ca, K, Cl, S and P (mg g^{-1} dry weight) of the samples (A to D correspond to femurs A to D in Fig. 1). These concentrations are obtained after correction for the local tissue density using H, C, N and O. The Ca and P concentrations are scaled such that the gradients in the growth plate become visible. As a result, the peak values in the bone are not visible. Distinct gradients in Ca, K, Cl and S slowly develop with maturation of the growth plate from sample A to D. They are most clearly visible in sample C. Owing to the presence of the secondary ossification centre at the left side in sample D, gradients develop in both directions.

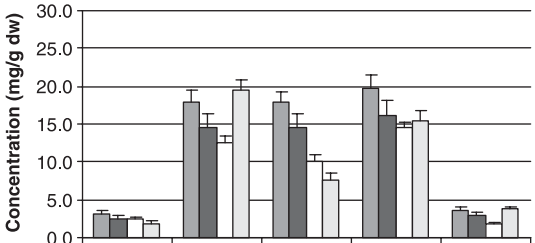

	P	S	Cl	K	Ca
A	3.1	17.9	17.9	19.8	3.6
B	2.5	14.6	14.6	16.1	2.9
C	2.4	12.6	10.1	14.5	1.8
D	1.8	19.6	7.7	15.4	3.8

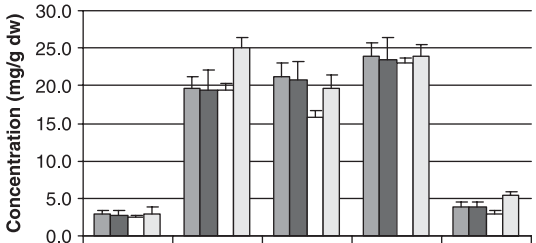

	P	S	Cl	K	Ca
A	2.8	19.5	21.1	23.8	3.9
B	2.8	19.4	20.9	23.6	3.9
C	2.5	19.3	15.8	22.9	2.9
D	3.0	25.0	19.7	23.8	5.4

Fig. 4 Average element concentrations in the four samples (A–D) in the proliferative (left) and hypertrophic (right) zones over areas 350–550 μm (left) and 650–950 μm (right) as indicated in Fig. 3. These areas are selected because they are parts of, respectively, the proliferative and hypertrophic zones in all animals. The only exception is for the concentrations of Cl and K in the hypertrophic zones in animals C and D. Because these elements develop steep gradients towards the mineralized area (Fig. 3C,D), they are averaged over 105–107 μm (animal C) and 98–100 μm (animal D).

maturation of the growth zone. When the primary ossification centre has fully developed (Fig. 3C), a peculiar step-wise increase in the concentrations of K and S is present at the transition between resting zone and proliferative zone, which is at a distance of approximately 450 μm from the ossification front. Interestingly, the step-wise gradient in S develops because its concentration decreases with maturation in the reserve zone, while it remains at the same level in the more active proliferative and hypertrophic zones. In the oldest animal, S and K increase towards both sides (Fig. 3D). The concentration profile of Cl resembles that of S in the youngest animals (Fig. 3A,B), but then develops into a distinct pattern characterized by a steep rise in concentration in the hypertrophic zones (Fig. 3C,D).

To enable quantitative comparison of element concentrations between zones in the developing bones, averaged values for the resting zone and the differentiating part of the tissue were computed (Fig. 4). All values are averages over the regions between 350–550 μm and 650–950 μm, respectively (location can be identified on the *x*-axis in Fig. 3). The only exception is for the concentrations of Cl and K in the hypertrophic zones in animals C and D. Because these elements develop steep gradients towards the mineralized area (Fig. 8C,D), they are averaged over 105–107 μm (animal C) and 98–100 μm (animal D). Interestingly, with maturation of the bone the concentrations of these elements tended to decrease in the resting zone, whereas they remained rather constant with age in the rest of the tissue (Fig. 4).

Discussion

Concentration profiles of Ca, P, S, Cl and K were obtained from PIXE measurements on growth zones of fetal porcine bones of different ages. In combination with measurements of local H, N, C and O by FS and RBS the local tissue dry weight was determined, which enabled quantification of element concentrations. The profiles show how concentration gradients of Ca, S, K and Cl develop with maturation of the bone, while the concentration of P remains constant throughout the tissue. A small gradient of P starts to develop at a later stage of development.

The average concentration of Ca in a developed growth zone (femur C) is 1.75 ± 0.21 mg g^{-1} dw in the resting zone and gradually increases to 2.9 ± 0.4 mg g^{-1} dw in the hypertrophic zone (Fig. 4). Ca concentration shows a steeper profile in the terminal hypertrophic zone, increasing from 2.9 ± 0.4 to 4.6 mg g^{-1} dw within the last 60 μm prior to calcification (Fig. 3C). Using scanning transmission electron microscopy (STEM) it was found that the concentration of Ca increased from 2.0 mg g^{-1} dw in the resting zone to 3.1 mg g^{-1} dw in the proliferative and 3.9 mg g^{-1} dw in the hypertrophic zone of rat rib growth plates (Wroblewski, 1987). This concurs quantitatively with our data. Note that the steep gradient in Ca concentration in the late hypertrophic zone could not be detected in the experiment by Wroblewski (1987). A similar gradient in free Ca concentration was found by Mwale et al. (2002). Unfortunately, quantitative comparison is impossible because the latter data are based on wet tissue weight.

Once a secondary ossification centre has developed, the average concentration of Ca throughout the growth plate increases from 2.2 ± 0.6 mg g^{-1} dw (femur C) to 4.8 ± 0.9 mg g^{-1} dw (femur D) (Fig. 4). As for femur C (Fig. 3C), the Ca concentration in femur D increases from the resting zone (3.8 ± 0.4 mg g^{-1} dw; Fig. 4) to the hypertrophic zone (5.4 ± 0.5 mg g^{-1} dw; Fig. 4). A similar steep gradient towards the secondary ossification centre is apparent in femur D, where the concentration of Ca increases by ~2 mg g^{-1} dw within the final 60 μm of the late hypertrophic zone (Fig. 3D). Why this gradient seems absent in femur D near the primary ossification centre is unclear. One may speculate that enhanced chondrocyte maturation in femur D compared with femur C, as possibly indicated by the simultaneous increase in Cl concentration in this zone, results in loss of Ca. Another possibility is that bone turnover is reduced at the time the secondary ossification centre forms. The associated reduced osteoclastic bone resorption may lower the Ca^{2+} concentration in the bone and hence the Ca gradient close to the interface between bone and cartilage. The average increase in Ca concentration throughout the growth zone between femurs C and D is hypothesized to result from overlapping Ca gradients from both sides once the secondary ossification centre has developed. This indicates that the Ca gradient is the result of a transport process starting in the mineralized area. As a result, it is anticipated that the concentration of Ca in the resting zone increases with narrowing of the growth plate. Given the importance of Ca for cell maturation, we speculate that a similar effect may contribute to the eventual closure of the growth plate.

Like the Ca profile, the Cl and K concentrations (Fig. 3C) averaged per resting, proliferative and hypertrophic zone concur with the literature (Wroblewski, 1987). Some quantitative differences – our data are slightly higher on average – may reflect differences between growth plates and species. Alternatively, Wroblewski (1987) may have overestimated their slice thickness. The STEM technique requires this estimate to derive concentration data. An additional assumption with STEM is that the amount of H, C, N and O is similar throughout the tissue, which is questionable in the strongly differentiating tissue studied herein. The presently used method corrects for H, C, N and O concentrations for each measurement spot. Therefore, this method produces definite concentrations throughout the tissue.

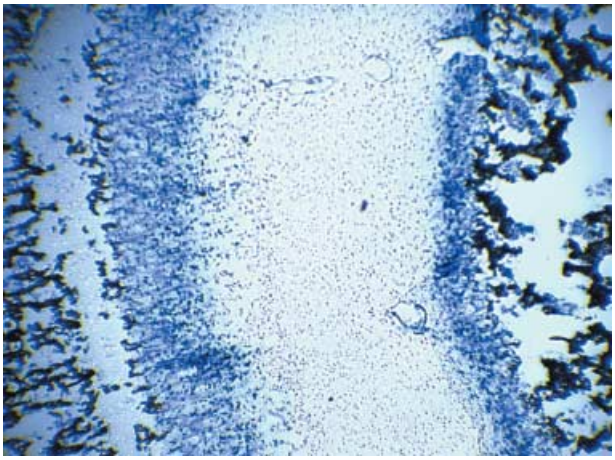

Fig. 5 Alkaline phosphatase (blue) in the hypertrophic zones of a growth plate of a late fetal porcine bone (sample 4). Left: primary ossification centre; right: secondary ossification centre. The distributions of most elements under consideration show a similar asymmetric distribution over a growth plate at this stage of development (Fig. 3D).

There is a mismatch in P and S concentrations between the present measurements and those of Wroblewski (1987). In our measurements, the average P concentration in the resting zone of the growth plate in animal C was 2.4 ± 0.3 mg g^{-1} dw and 2.5 ± 0.3 mg g^{-1} dw in the differentiating tissue. No P concentration gradient is apparent (Figs 3C and 4). From the resting zone to the hypertrophic zone, Wroblewski found an increase from 2.2 to 4.0 mg g^{-1} dw in the matrix and from 20.5 to 28.6 mg g^{-1} dw in the cells. The most developed sample in the present study shows the onset of a P gradient, suggesting a P gradient may develop at a later stage of development (Fig. 3D).

Interestingly, free Pi increases five-fold from the early proliferative to the late hypertrophic zone (Mwale et al. 2002), whereas the P concentration does not change (Fig. 3C) or shows a significantly less than five-fold increase (Fig. 3D and Wroblewski, 1987). Assuming that P is predominantly present as phosphate, we hypothesize that sufficient phosphate is present throughout the growth plate, but that the ratio of unbound/bound phosphate increases towards the zone of calcification. The activity of dephosphorylating enzymes such as alkaline phosphatase, abundantly expressed by hypertrophic chondrocytes (Fig. 5), is required for increasing the free Pi concentration in the tissue. This indicates that diffusion from the ossified

area into the growth plate is probably not as effective for Pi as it is for Ca. It would be interesting to study this hypothesis using a method that can distinguish between differences in chemical binding states, which is not possible with the currently employed technique.

The steep step-wise increase in S between resting (12.6 ± 0.8 mg g^{-1} dw; Fig. 4) and proliferative (19.3 ± 0.9 mg g^{-1} dw; Fig. 4) zones of mature growth plates has not previously been shown. The same holds for the clear development of this step with maturation of the growth plate. Quantitatively, the S concentrations from the resting and hypertrophic zones compare well with previous STEM measurements at small spots in these zones (14.5 and 26.4 mg g^{-1} dw, respectively) (Wroblewski, 1987). Their higher concentration of 37.7 mg g^{-1} dw locally in the proliferative zone is not confirmed here. We have confidence in our data because S, which is assumed to represent the distribution of negatively charged sulphated proteoglycans, corresponds closely with the profile of positively charged K ions.

The Cl concentration shows a steep gradient close to the mineralized area, co-localizing with the hypertrophic zone. In the situation where the secondary ossification centre has developed (Fig. 3D) the zone with increased Cl signal is smaller close to the secondary ossification centre than near the primary ossification centre. This dissimilarity is present in the size of the hypertrophic zone as well, as revealed by expression of alkaline phosphatase (Fig. 5). It is possible that an excessive increase in intracellular chloride concentration during hypertrophy is responsible for the increase in chloride concentration.

In conclusion, we confirm earlier findings that a Ca concentration gradient towards the mineralized area exists. This gradient is thought to be important for chondrocyte maturation and is likely to result from a diffusive process. In addition, we show for the first time the development of this gradient with tissue maturation. We have not detected a P gradient during the early developmental stages when other gradients are already present. This suggests to us that the increase of free Pi towards the bone-forming site (Mwale et al. 2002) results from an enzymatic controlled transition of phosphate from a bound to an unbound state, rather than being the result of diffusion. Finally, the onset of proliferation is co-localized with a step-wise increase in S, which clearly develops over time with tissue maturation.

Acknowledgement

We gratefully acknowledge Ballering Export C.V. (Eindhoven, The Netherlands) for providing the porcine embryos.

References

Alini M, Carey D, Hirata S, Grynpas MD, Pidoux I, Poole AR (1994) Cellular and matrix changes before and at the time of calcification in the growth plate studied in vitro: arrest of type X collagen synthesis and net loss of collagen when calcification is initiated. *J Bone Miner Res* **9**, 1077–1087.

Bonen DK, Schmid TM (1991) Elevated extracellular calcium concentrations induce type X collagen synthesis in chondrocyte cultures. *J Cell Biol* **115**, 1171–1178.

Brands PJM, Mutsaers PHA, De Voigt MJA (1999) System for on-line monitoring of light element concentration distributions in thin samples. *Nuclear Instruments and Methods in Physics Research, Section B: Beam Interactions with Materials and Atoms* **158**, 135–140.

Burton DW, Foster M, Johnson KA, Hiramoto M, Deftos LJ, Terkeltaub R (2005) Chondrocyte calcium-sensing receptor expression is up-regulated in early guinea pig knee osteoarthritis and modulates PTHrP, MMP-13, and TIMP-3 expression. *Osteoarthritis Cartilage* **13**, 395–404.

Byers S, van Rooden JC, Foster BK (1997) Structural changes in the large proteoglycan, aggrecan, in different zones of the ovine growth plate. *Calcified Tissue Int* **60**, 71–78.

Cecil DL, Rose DM, Terkeltaub R, Liu-Bryan R (2005) Role of interleukin-8 in PiT-1 expression and CXCR1-mediated inorganic phosphate uptake in chondrocytes. *Arthritis Rheum* **52**, 144–154.

Chu W-K, Mayer JW, Nicolet M-A (1978) *Backscattering Spectrometry*, 1st edn. Orlando, FL: Academic Press.

Fujii T, Takai S, Arai Y, Kim W, Amiel D, Hirasawa Y (2000) Microstructural properties of the distal growth plate of the rabbit radius and ulna: biomechanical, biochemical, and morphological studies. *J Orthopaedic Res* **18**, 87–93.

Gakunga PT, Kuboki Y, Opperman LA (2000) Hyaluronan is essential for the expansion of the cranial base growth plates. *J Craniofacial Genet Dev Biol* **20**, 53–63.

Hunziker EB, Schenk RK (1989) Physiological mechanisms adopted by chondrocytes in regulating longitudinal bone growth in rats. *J Physiol* **414**, 55–71.

Isabelle DB (1994) The pixe analytical technique: principle and applications. *Radiation Physics Chem* **44**, 25–30.

Johansson SAE (1989) PIXE: a novel technique for elemental analysis. *Endeavour* **13**, 48–53.

Kirsch T, Swoboda B, Nah H (2000) Activation of annexin II and V expression, terminal differentiation, mineralization and apoptosis in human osteoarthritic cartilage. *Osteoarthritis Cartilage* **8**, 294–302.

Kronenberg HM (2003) Developmental regulation of the growth plate. *Nature* **423**, 332–336.

Lefebvre V, Smits P (2005) Transcriptional control of chondrocyte fate and differentiation. *Birth Defects Res Part C, Embryo Today: Reviews* **75**, 200–212.

Magne D, Bluteau G, Faucheux C, et al. (2003) Phosphate is a specific signal for ATDC5 chondrocyte maturation and apoptosis-associated mineralization: possible implication of apoptosis in the regulation of endochondral ossification. *J Bone Miner Res* **18**, 1430–1442.

Mansfield K, Rajpurohit R, Shapiro IM (1999) Extracellular phosphate ions cause apoptosis of terminally differentiated epiphyseal chondrocytes. *J Cell Physiol* **179**, 276–286.

Mansfield K, Teixeira CC, Adams CS, Shapiro IM (2001) Phosphate ions mediate chondrocyte apoptosis through a plasma membrane transporter mechanism. *Bone* **28**, 1–8.

Mansfield K, Pucci B, Adams CS, Shapiro IM (2003) Induction of apoptosis in skeletal tissues: phosphate-mediated chick chondrocyte apoptosis is calcium dependent. *Calcified Tissue Int* **73**, 161–172.

der Mark K, Kirsch T, Nerlich A, et al. (1992) Type X collagen synthesis in human osteoarthritic cartilage. Indication of chondrocyte hypertrophy. *Arthritis Rheum* **35**, 806–811.

Mous DJW, Haitsma RG, Butz T, Flagmeyer RH, Lehmann D, Vogt J (1997) Novel ultrastable HVEE 3.5 MV Singletron accelerator for nanoprobe applications. *Nuclear Instruments and Methods in Physics Research, Section B: Beam Interactions with Materials and Atoms* **130**, 31–36.

Mutsaers PHA, Los G, Klein SS, De Folter LC, De Voigt MJA (1990) Microprobe at the Eindhoven University of technology. *Nuclear Instruments and Methods in Physics Research, Section B: Beam Interactions with Materials and Atoms* **45**, 557–560.

Mwale F, Tchetina E, Wu CW, Poole AR (2002) The assembly and remodeling of the extracellular matrix in the growth plate in relationship to mineral deposition and cellular hypertrophy: an in situ study of collagens II and IX and proteoglycan. *J Bone Miner Res* **17**, 275–283.

Noonan KJ, Hunziker EB, Nessler J, Buckwalter JA (1998) Changes in cell, matrix compartment, and fibrillar collagen volumes between growth-plate zones. *J Orthopaedic Res* **16**, 500–508.

Ortega N, Behonick DJ, Werb Z (2004) Matrix remodeling during endochondral ossification. *Trends Cell Biol* **14**, 86–93.

Radhakrishnan P, Lewis NT, Mao JJ (2004) Zone-specific micromechanical properties of the extracellular matrices of growth plate cartilage. *Ann Biomed Engineering* **32**, 284–291.

Reinert T, Butz T, Flagmeyer RH, et al. (1998) Investigation of the calcium content in joint cartilage: Is it connected with (early arthrotic) changes in cartilage structure? *Nuclear Instruments and Methods in Physics Research, Section B: Beam Interactions with Materials and Atoms* **136–138**, 936–940.

Shapses SA, Sandell LJ, Ratcliffe A (1994) Differential rates of aggrecan synthesis and breakdown in different zones of the bovine growth plate. *Matrix Biol* **14**, 77–86.

Tchetina EV, Squires G, Poole AR (2005) Increased type II collagen degradation and very early focal cartilage degeneration is associated with upregulation of chondrocyte differentiation related genes in early human articular cartilage lesions. *J Rheumatol* **32**, 876–886.

Traxel K (1998) Nuclear microprobes and their significance for trace element analysis. *Nuclear Instruments and Methods in Physics Research, Section A: Accelerators, Spectrometers, Detectors and Associated Equipment* **268**, 567–578.

Wada K, Mizuno M, Komori T, Tamura M (2004) Extracellular inorganic phosphate regulates gibbon ape leukemia virus receptor-2/phosphate transporter mRNA expression in rat bone marrow stromal cells. *J Cell Physiol* **198**, 40–47.

Wilsman NJ, Farnum CE, Leiferman EM, Fry M, Barreto C (1996) Differential growth by growth plates as a function of multiple parameters of chondrocytic kinetics. *J Orthopaedic Res* **14**, 927–936.

Wroblewski J (1987) Elemental changes associated with chondrocyte differentiation in rat rib growth plate. *Histochemistry* **87**, 145–149.

Wu CW, Tchetina EV, Mwale F, et al. (2002a) Proteolysis involving matrix metalloproteinase 13 (collagenase-3) is required for chondrocyte differentiation that is associated with matrix mineralization. *J Bone Miner Res* **17**, 639–651.

Wu LN, Guo Y, Genge BR, Ishikawa Y, Wuthier RE (2002b) Transport of inorganic phosphate in primary cultures of chondrocytes isolated from the tibial growth plate of normal adolescent chickens. *J Cell Biochem* **86**, 475–489.

Wu S, Palese T, Mishra OP, Delivoria-Papadopoulos M, De Luca F (2004) Effects of Ca^{2+} sensing receptor activation in the growth plate. *FASEB J* **18**, 143–145.

Zuscik MJ, D'Souza M, Ionescu AM, et al. (2002) Growth plate chondrocyte maturation is regulated by basal intracellular calcium. *Exp Cell Res* **276**, 310–319.